ELSEVIER

Materials Science and Engineering B77 (2000) 193–201

MATERIALS SCIENCE & ENGINEERING B

www.elsevier.com/locate/mseb

Synthesis of tungsten trioxide hydrates and their structural properties

M. Gotić [a], M. Ivanda [a], S. Popović [b], S. Musić [a,*]

[a] *Division of Materials Chemistry, Ruđer Bošković Institute, PO Box 180, Bijenička Cesta 54, 100012 Zagreb, Croatia*
[b] *Department of Physics, Faculty of Science, University of Zagreb, PO Box 331, 100012 Zagreb, Croatia*

Received 25 February 2000; accepted 24 May 2000

Abstract

Tungsten trioxide hydrates were synthesized by (a) cation exchange reaction from sodium tungstate solution and (b) precipitation from sodium tungstate solution by the addition of HCl solution. The samples were analyzed by XRD, DTA/TGA, Raman and FT-IR spectroscopy. XRD showed formation of $WO_3 \cdot H_2O$ by cation exchange reaction, whereas $WO_3 \cdot 0.33H_2O$ was identified by XRD as a product of the acidification of sodium tungstate solution with HCl solution. After heating at 320°C, $WO_3 \cdot H_2O$ transformed into WO_3, whereas the $WO_3 \cdot 0.33H_2O$ crystal structure remained and these results were in agreement with DTA/TGA measurements. The $WO_3 \cdot H_2O$ sample synthesized by cation exchange reaction showed a weight loss corresponding to one molecule of water in the crystal structure. However, samples $WO_3 \cdot 0.33H_2O$ showed a much greater weight loss upon heating than could be expected on the basis of the WO_3 $0.33H_2O$ formula. The phase transition $WO_3 \cdot H_2O \rightarrow WO_3$ was also monitored by Raman and FT-IR spectroscopy. In the case of $WO_3 \cdot 0.33H_2O$ samples, the basic features of Raman and FT-IR spectra did not change on heating to 320°C, thus indicating that the heating of $WO_3 \cdot 0.33H_2O$ up to this temperature did not destroy the original crystal structure. Contrary to this, after heating the $WO_3 \cdot H_2O$ sample to 320°C, the Raman and FT-IR spectra showed a series of new bands caused by the phase transition $WO_3 \cdot H_2O \rightarrow WO_3$.

Keywords: Tungsten trioxide hydrates; Cation exchange reaction; Raman spectroscopy

1. Introduction

Numerous publications about possible, as well as actual, applications of tungsten oxide, WO_3, and its hydrates were published in the last decade. The electrochromic properties of WO_3 and its hydrates were extensively investigated [1–9]. The electrochromic properties of WO_3 can be modified by insertion of Li^+ ions into material in accordance with the reaction [10]:

$$x\,Li^+ + x\,e^- + WO_3 \rightarrow Li_x W^{(VI)}_{1-x} W^{(V)}_x O_3$$

Tungsten oxides also found in important applications in catalysis. In these applications tungsten oxides are mainly used as coatings on various inorganic oxide substrates. These oxide substrates include Al_2O_3 [11,12], TiO_2 [13,14], TiO_2–Al_2O_3 [15], ZrO_2 [16] and SiO_2 [17,18]. Possible application of the WO_3 film in a surface acoustic wave gas sensor was also investigated [19].

The chemical and physical properties of metal oxides, including tungsten oxide, are generally dependent on the route of their synthesis. Knowledge of the relation between the synthesis conditions of specific metal oxide and its functional properties is important for the possible application of metal oxides in advanced technologies. Tungsten oxide and its hydrates can be synthesized using various chemical methods, such as 'wet' chemical precipitation, hydrolysis of tungsten alkoxide or thermal decomposition of tungsten salts. The WO_3 films on various substrates can also be prepared using various vacuum techniques. Modification of the chemical or physical route within the same method also influences the resulting properties of the synthesized material.

In the present work we have focused on the 'wet' chemical precipitation of tungsten trioxide hydrates and determination of their structural properties and thermal behaviors. Since the 'wet' chemical precipitation

* Corresponding author.

0921-5107/00/$ - see front matter
PII: S0921-5107(00)00488-8

method is very sensitive to the physicochemical conditions of the precipitation, the experimental parameters in the chemical synthesis were thoroughly controlled. Tungsten trioxide hydrates were synthesized (a) by cation exchange reaction from sodium tungstate solution and (b) by acidification of the sodium tungstate solution. The cation exchange reaction generates a sodium and chloride free solution with a lot of possibilities for chemical and morphological modifications.

2. Experimental

Dowex® 50W-X (20–50 mesh) a cation exchange resin with large effective pore size, (Bio-Rad Laboratories), $Na_2WO_4 \cdot 2H_2O$, (Analytical Reagent, B.D.H. Lab. Chem. Division), HCl and NaOH (p.a.) and doubly distilled water were used.

2.1. Sample W 1

Dowex cation exchange resin in hydrogen form (70 g) was swelled in a doubly distilled water. Then the resin grains were transferred in a glass column and washed successively with a doubly distilled H_2O, 2 M NaOH, doubly distilled H_2O, 1 M HCl and again with doubly distilled H_2O. Through such a prepared cation exchange column, a 0.1 M Na_2WO_4 solution was passed, yielding a clear and stable tungstate solution. The measured pH of the solution after its passing through the Dowex column was 3.0–3.5. In order to increase the polymerization of tungstate anion, a clear solution thus obtained was autoclaved at 60°C for 72 h. Due to a relative high pH, the solution remained clear, and for this reason the same solution was additionally passed twice through the Dowex resin column which gave a clear solution having pH 1.8. The solution was kept in a closed flask and shaken properly for 30 min. A white–yellow precipitate appeared within 2 h. The colloidal solution was left in the closed flask at room temperature for 40 h. An intense green–yellow precipitate was formed. It was isolated by decantation and centrifugation, washed twice with doubly distilled H_2O and then dried in a Petri dish at 60°C for 48 h. The sample was denoted as W1.

2.2. Sample W 2

HCl (150 ml, 0.7 M) was carefully added to 500 ml of 0.1 M Na_2WO_4 solution until the final pH of the clear solution reached a value of 1.6. The clear solution thus obtained was autoclaved at 60°C for 48 h. A white precipitate appeared within 1 h. After 48 h of autoclaving the white precipitate was isolated by decantation and centrifugation, washed several times with doubly distilled water and then dried in a Petri dish at 60°C for 48 h. The color of this sample did not change from first appearance to its isolation. The sample was denoted as W2.

2.3. Sample W 3

The 1.0 M Na_2WO_4 solution was used, instead of the 0.1 M Na_2WO_4 solution, 300 ml of 0.7 M HCl were added to 100 ml of the 1.0 M $Na_2WO_4 \cdot 2H_2O$ solution until the final pH of a clear solution reached a value of 1.4. The solution obtained was autoclaved at 60°C for 48 h and then isolated by centrifugation. White precipitate was washed several times with doubly distilled H_2O and then dried in a Petri dish at 60°C for 48 h. The sample was denoted as W3.

2.4. Thermally treated samples

Samples $W1_{320}$, $W2_{320}$ and $W3_{320}$ were obtained by thermal treatment of samples W1, W2 and W3 at 320°C in a tubular furnace with a temperature stability of ± 30°C. Samples $W3_{600}$ and $W3_{800}$ were obtained by thermal treatment of sample W3 at 600 and 800°C, respectively.

X-ray powder diffraction patterns were taken at room temperature (25°C) using a Philips MPD 1880 diffractometer with monochromatized Cu–Kα radiation (graphite monochromator).

Thermal analysis was performed using an instrument manufactured by Netzsch. The temperature was controlled by a Pt–PtRh (10%) thermocouple, by applying a heating rate of 10°C min^{-1} (DTA) and 5°C min^{-1} (TGA).

The Raman scattering experiments were performed in the back scattering configuration using the line focusing technique [20]. A coherent Innova-100 laser with $\lambda = 514.5$ nm was used as the excitation source. The energy of the laser light was small enough to avoid possible damage to the samples. The scattering light was analyzed with a DILOR Z-24 Raman spectrometer.

The FT-IR spectra were recorded at room temperature using a Perkin–Elmer spectrometer (model 2000). The IRDM (Infrared Data Manager) program, supplied by Perkin–Elmer, was used to process the spectra. Infrared spectra of the samples pressed into KBr pellets were collected in the wave number range of 4000–400 cm^{-1} (mid-IR region) using a KBr beamsplitter. Powder samples measured in the wave number range of 700–100 cm^{-1} (far-IR region) were gently mixed with spectroscopically pure polyethylene powder, pressed into pellets and recorded in a compartment purged with extra pure nitrogen using a Mylar beamsplitter. At least 100 scans with a resolution of 4 cm^{-1} in the far-IR region were accumulated.

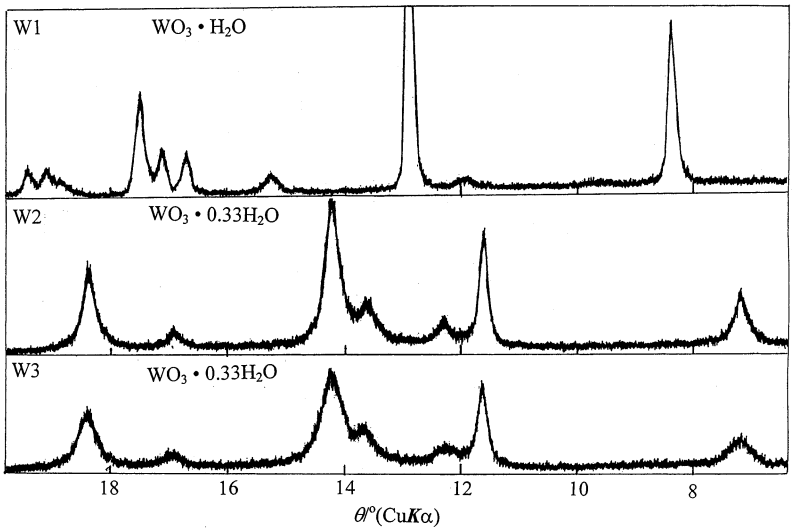

Fig. 1. Characteristic parts of XRD patterns of samples W1, W2 and W3 recorded at room temperature.

3. Results and discussion

3.1. X-ray powder diffraction and thermal analysis data

Fig. 1 shows characteristic X-ray powder diffraction patterns of samples W1, W2 and W3, whereas Table 1 contains reference data [21] used for identification of crystalline phases. Sample W1, corresponding to $WO_3 \cdot H_2O$, shows a small broadening of the diffraction lines. The $WO_3 \cdot 0.33H_2O$ structure is found in samples W2 and W3. Broadening of diffraction lines is observed for sample W2, whereas sample W3 shows very broadened lines, thus indicating a smaller crystallite size than in sample W2. On heating samples W1, W2 and W3 at 320°C, sample W1 turns into WO_3 by releasing one H_2O molecule, whereas in samples W2 and W3, the $WO_3 \cdot 0.33H_2O$ structure is preserved.

Differences in temperature of the WO_3 formation arise from the structure of the WO_3 precursor. For example, Nishide and Mizukami [22] prepared WO_3 films which were subjected to heating up to 700°C. The Raman spectra indicated that amorphous WO_3 was obtained up to 300°C for the films on silicon wafers, prepared with or without complexing agent 2,4-pentanedione. Crystallization occurred between 300 and 500°C. Cubic WO_3 alone was formed on the quartz glass substrates when the films were prepared in the presence of the complexing agent and heated between 500 and 700°C. Li et al. [23] used FT-IR emission spectra and DTA curves to investigate the thermal decomposition of ammonium tungstate salt. FT-IR emission spectra showed that the salt was entirely decomposed into WO_3 at $\sim$400°C, and a very strong and broad IR band at 890 cm^{-1} was assigned to WO_3. DTA showed two endothermic peaks at 139 and 3300°C, which were related to the decomposition of the ammonium ions, whereas the exothermic peaks at 250 and 400°C were related to the loss of crystalline water and formation of a WO_3 phase, respectively.

The DTA curve of sample W1, which was synthesized by a cation exchange reaction, is shown in Fig. 2. Sample W1 is characterized by a relatively broad endothermic peak at 265°C and a relatively small exothermic peak at 315°C. The endothermic peak at 265°C could be attributed to the elimination of structurally bonded water molecules, whereas the exothermic peak at 315°C corresponds to the phase transition from $WO_3 \cdot H_2O$ to WO_3. DTA curves of samples W2 and W3 (Fig. 2) differ significantly from those of sample W1, and they are characterized by two exothermic peaks of different relative intensity at 480 and 490°C and with one relatively small endothermic peak at 735°C. Exothermic peaks at 480 and 490°C of samples W2 and W3 can be related to the phase transition from the $WO_3 \cdot 0.33H_2O$ into the WO_3 structure. Due to the

Table 1
XRD phase analysis of the samples

Sample	XRD analysis of the sample	PDF[21] card no.
W1	$WO_3 \cdot H_2O$	43-679
W2	$WO_3 \cdot 0.33H_2O$	35-1001 35-270
W3	$WO_3 \cdot 0.33H_2O$	35-1001 35-270
$W1_{320}$	WO_3	32-1395 43-1035
$W2_{320}$	$WO_3 \cdot 0.33H_2O$	35-1001 35-270
$W3_{320}$	$WO_3 \cdot 0.33H_2O$	35-1001 35-270

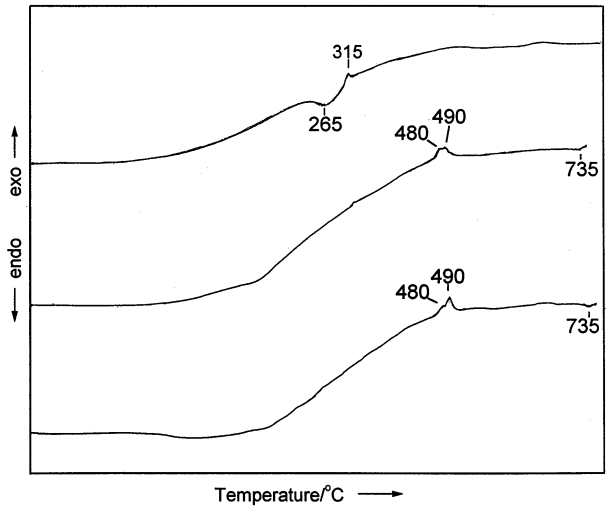

Fig. 2. DTA curves of samples W1, W2 and W3.

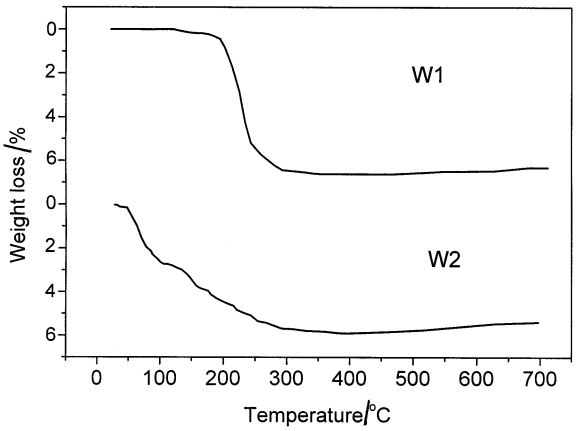

Fig. 3. TGA curves of samples W1 and W2.

presence of Cl^- ions during the precipitation process and their possible incorporation into the hydrated tungsten oxide structure, it appears that the phase transition from hydrated WO_3 into anhydrous WO_3 is a more complex process that occurs at a much higher temperature compared with the same phase transition for the material obtained by cation exchange. These DTA findings are in accordance with XRD results which showed that W1 samples thermally treated at 320°C changed phase composition, while W2 and W3 samples thermally treated at the same temperature did not change their phase composition.

The endothermic peak observed at 735°C for samples W2 and W3 could not be ascribed with certainty only to residual OH^- groups in these samples. For this reason, sample W3 was heated up to 600 or 800°C. XRD analysis of the sample produced at 600°C showed the presence of monoclinic WO_3 and two minor phases, not identified using PDF [21]. The sample produced at 800°C showed, besides monoclinic WO_3, the presence of only one of two minor phases, which contained the sample produced at 600°C. A gradual sharpening of diffraction lines corresponding to monoclinic WO_3 was observed for the samples obtained between 320 and 800°C.

Thermal analysis confirmed significant structural and physical differences among W1, W2 and W3 samples. Fig. 3 shows TGA curves of samples W1 and W2. TGA of samples W1, W2 and W3 was performed between room temperature and 713, 694 and 727°C, respectively, with a heating rate of 5°C min^{-1}. The TGA curve of sample W1 showed a very flat region between room temperature and 178°C, so it can be inferred that no weight loss occurs until 178°C. Weight loss in sample W1 starts at 178°C and is completed at 384°C. There is no other weight loss between 384°C and the final heating temperature at 713°C. The total weight loss for sample W1 corresponded to the value of 6.63 wt.%, and this value is in good agreement with the phase composition $WO_3 \cdot H_2O$ (theoretical amount of water 7.20 wt.%) as determined by XRD. On the basis of the TGA results it can be concluded that sample W1 did not possess physically adsorbed water. Contrary to this result, for samples W2 and W3 the weight loss starts at 42°C and completes at 384°C, i.e. in a much broader temperature region compared with sample W1. The total weight loss for samples W2 and W3 corresponds to the values 5.72 and 6.29 wt.%, respectively. These values are much greater than would be expected on the basis of theoretical weight loss, due to the released water molecules structurally present in the $WO_3 \cdot 0.33H_2O$ phase.

Significantly different thermal behavior between sample W1 on one hand and samples W2 and W3 on the other can be explained by their different chemical synthesis routes. Sample W1 was synthesized by a cation exchange reaction, which enabled the polymerization on molecular level in a cation- and anion-free medium. Generally, inorganic polymerization in acidic conditions as the synthesis route for obtaining metal oxides involves several stages, such as the formation of metal hydroxy complexes, formation of hydroxy polymers (olation), formation of oxobridges (oxolation) and, finally, a visible solid product. Counter anions such as Cl^-, NO_3^-, SO_4^{2-}, etc. strongly influence the polymerization process, and thus the final solid product [24,25]. An influence of anion counter ions on the chemical and physical properties of the final product was also shown in the present work. Sample W3 synthesized in the presence of a greater content of chlorides has shown a more continuous and greater weight loss (6.29 wt.%) than sample W2 (5.72 wt.%). Generally, the structural water in tungsten trioxide is one of the most important factors for the preparation of a good photochromic material.

Figlarz and co-workers [26,27] also investigated thermal behavior of $WO_3 \cdot 0.33H_2O$. DSC measurement

showed a first endothermic peak at ~80°C due to desorption of water, and the second endothermic peak at 350°C due to dehydration of water. The first exothermic peak at ~400°C was ascribed to the supermetastable $WO_3 \rightarrow$ metastable hexagonal WO_3 transformation, whereas a second exothermic peak at ~500°C was ascribed to the transformation of hexagonal WO_3 into monoclinic WO_3. These transformations can be described with the following scheme:

$$WO_3 \cdot 0.33H_2O \rightleftarrows \text{supermetastable } WO_3$$
$$\rightarrow \text{hexagonal } WO_3 \rightarrow \text{monoclinic } WO_3$$

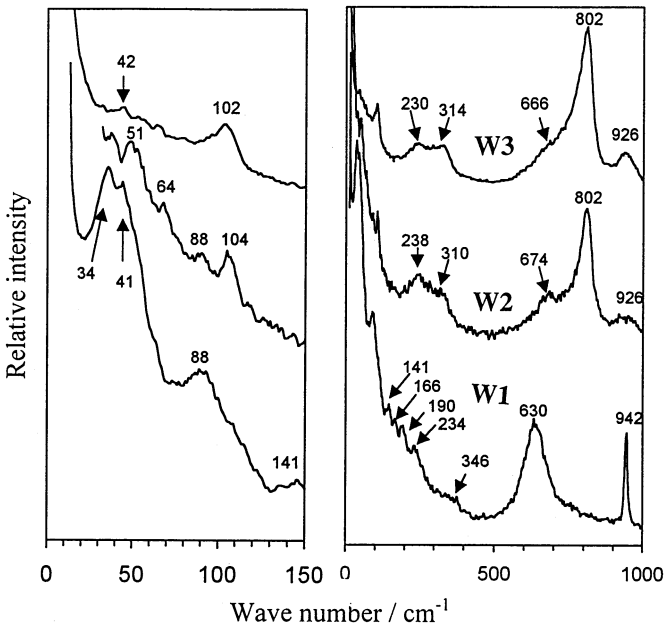

Fig. 4. Laser Raman spectra of samples W1, W2 and W3 recorded at room temperature.

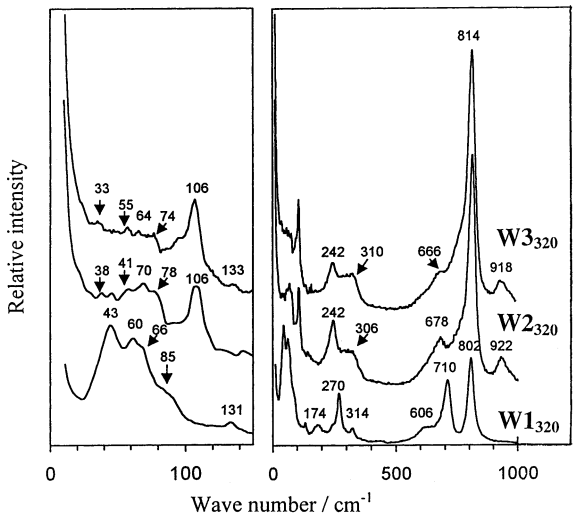

Fig. 5. Laser Raman spectra of samples $W1_{320}$, $W2_{320}$ and $W3_{320}$ recorded at room temperature.

Formation of WO_3 polymorphs and their structural stability are very dependent on the experimental conditions. Laruelle and Figlarz [28] prepared hexagonal WO_3 by dehydration of $WO_3 \cdot 0.33H_2O$, and this WO_3 polymorph could be amorphized by high-energy ball milling. The same effect was observed for WO_3 with a pyrochlore-type structure. Monoclinic WO_3 was not amorphized in these experimental conditions; the effect of high-energy ball-milling was to decrease the crystallite size of monoclinic WO_3 to a limit value.

The polymorphism of the WO_3 powder sample, resulting from mild mechanical treatments and from temperature changes between 30 K and room temperature, has been investigated by Cazzanelli et al. [29]. Recently, Vogt et al. [30] investigated high-temperature phases of WO_3 between room temperature and 850°C. Two phases were found and characterized by Rietveld refinements: orthorhombic β-WO_3 at 350°C and tetragonal α-WO_3 at 800°C. Woodward et al. [31] reported the formation of WO_3 polymorphs upon heating: monoclinic (ε-WO_3) → triclinic (δ-WO_3) → monoclinic (γ-WO_3) → orthorhombic (β-WO_3) → tetragonal (α-WO_3).

3.2. Raman spectroscopy

Raman spectra of the samples investigated are shown in Figs. 4 and 5. The spectrum of sample W1 (Fig. 4) is characterized by a sharp Raman band at 942 cm^{-1}, a very strong and broad band at 630 cm^{-1} and a small intensity band at 346 cm^{-1}. The band at 942 cm^{-1} can be ascribed to the stretching mode of the terminal W=O bond, whereas the band at 630 cm^{-1} can be related to the vibration of the bridging oxygens. In the case of *m*-WO_3 two separate Raman bands at 807 and 715 cm^{-1} corresponding to the stretching vibrations of the bridging oxygens, were recorded by Daniel et al. [32]. The Raman band centered at 346 cm^{-1} can be ascribed to the $\nu(W–OH_2)$ vibrations. For the same vibrational mode in $WO_3 \cdot H_2O$, a Raman band at ~370 cm^{-1} is observed [32]. This difference can be explained by differences in the coordination conditions of H_2O molecules. In the low-frequency region, corresponding to the lattice vibration modes, several Raman bands are observed for sample W1. Also, an intensive Raman band with peaks at 34 and 41 cm^{-1} as well as bands centered at 88, 141, 166, 190 and 234 cm^{-1} were observed. Particle sizes are likely to produce spectral distortions, shifts, broadening and appearance of the so-called low-frequency Raman band. Ivanda et al. [33] elaborated the effect of particle size on the low-frequency Raman spectrum of metal oxides.

Heating of sample W1 at 320°C generated marked changes in the corresponding Raman spectrum, as shown in Fig. 5. For example, the band at 942 cm^{-1} disappeared and two separate bands at 802 and 710 cm^{-1} were formed due to the vibrations of the bridging

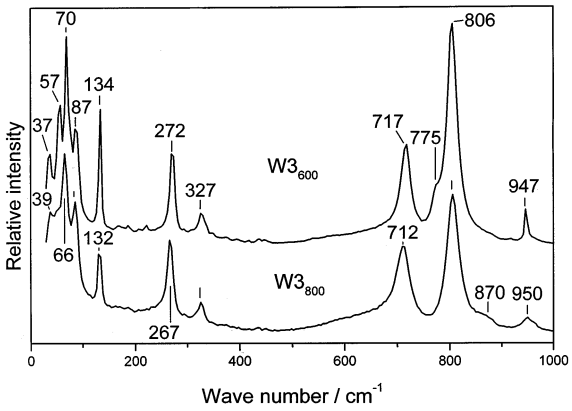

Fig. 6. Laser Raman spectra of samples $W3_{600}$ and $W3_{800}$.

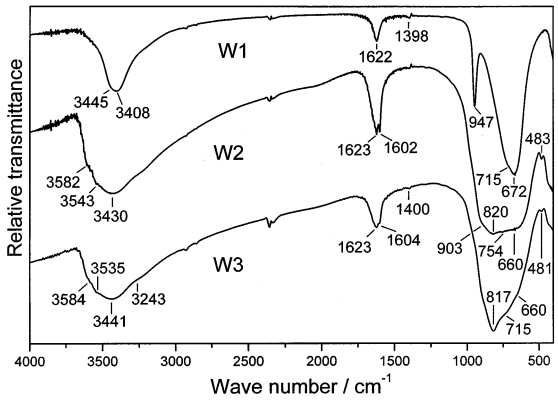

Fig. 7. Fourier transform infrared spectra of samples W1, W2 and W3, recorded at room temperature. Specimens were pressed into the KBr matrix.

oxygens. A shoulder at 606 cm^{-1} is also visible, and probably, this shoulder can be related to the Raman band at 630 cm^{-1} as observed for sample W1. This can be taken as an indication that the phase transition $WO_3 \cdot H_2O \rightarrow WO_3$ was not completed at 320°C. The band at 270 cm^{-1} can be assigned to δ(O–W–Ó) vibrations. In the low frequency region very strong and broad bands at 43 and 60 cm^{-1} with shoulders at 66 and 85 cm^{-1} and bands of small intensities at 131 and 174 cm^{-1} are recorded. The positions of Raman bands recorded at 43, 60, 65, 85 and 131 cm^{-1} are close to those published by Salje for WO_3 [34]. Wadayama et al. [35] investigated electrobleaching of WO_3 films prepared by vacuum deposition onto a platinum plate. On heating at 400°C the Raman bands at 805, 715 and 280 cm^{-1}, typical of *m*-WO_3, were recorded. Raman bands at 802 and 716 cm^{-1} were used [36] to monitor oxygen exchange between the yellow WO_3 and blue W_2O_5 and the surrounding gas phase, and it was found that the oxygen exchange was completely reversible, with molecular oxygen being the only gas phase involved chemically. In their synthesis [36] a commercial WO_3 was used with $\sim$10 μm particles.

Raman spectra of samples W2 and W3 (Fig. 4) are similar. The spectrum of sample W2 is characterized by a small intensity Raman band at 926 cm^{-1} due to the ν(W=O) vibrations, a very strong and broadened band at 802 cm^{-1} and a small intensity band at 674 cm^{-1}. The bands at 802 and 674 cm^{-1} can be ascribed to the vibrations of bridging oxygens in accordance with previous discussion, whereas a broad band with peaks centered at 310 and 238 cm^{-1} is located in the region of the ν(W–OH_2), δ(O–W–O) and ν(W–O–W) vibrations. In the low-frequency region the Raman bands at 104, 88, 64 and 51 cm^{-1} are recorded for sample W2, whereas a pronounced band at 102 cm^{-1} and a small intensity band at 42 cm^{-1} are observed for sample W3. On heating samples W2 and W3 at 320°C the corresponding Raman spectra (Fig. 5) showed the main spectral features of $WO_3 \cdot 0.33H_2O$. The dominant Raman band at 814 cm^{-1} was less broadened and the other Raman bands were better pronounced. Also, in the low-frequency region (Raman bands at 106, 78, 70, 41 and 38 cm^{-1}) the spectral similarity of samples $W2_{320}$ and $W3_{320}$ is visible. The Raman spectra of samples W2, W3 and $W2_{320}$ did not show a sharp band at 416 cm^{-1} ascribed to the δ(O–W–O) bending vibrations in $WO_3 \cdot 0.33H_2O$, as observed by other researchers [37,38].

Fig. 6 shows Raman spectra of samples $W3_{600}$ and $W3_{800}$, which were produced by heating the sample W3 up to 600 and 800°C. These spectra show a main feature of monoclinic WO_3. The Raman bands in the low-frequency region are more sharpened then those observed for WO_3 samples produced at lower temperatures; for example, as shown in Fig. 4 for sample $W1_{320}$.

3.3. FT-IR spectroscopy

The results of FT-IR spectroscopic measurements are shown in Figs. 7–10. Fig. 7 shows a mid-IR region for samples W1, W2 and W3, whereas the corresponding spectra recorded in the far-IR region are shown in Fig. 8. The spectrum of sample W1 shows a strong IR band located at 3408 cm^{-1} due to the stretching modes of OH groups and a band at 1622 cm^{-1} due to water molecules. A sharp IR band at 947 cm^{-1} and a very strong and broad band at 672 cm^{-1}, which are also Raman active, can be ascribed to the ν(W=O) and ν(O–W–O) vibrations, respectively. The FT-IR spectrum of sample W1, recorded in the far-IR region (Fig. 8), shows a band at 369 cm^{-1} with a shoulder at 393 cm^{-1} a band at 333 cm^{-1} and a band with peaks at 272 and 246 cm^{-1}. These IR bands are located in the region of the corresponding ν(W–OH_2), δ(O–W–O) and ν(W–O–W) vibrations. Additionally, a band at $\sim$176 cm^{-1} is visible and this band can be ascribed to the lattice modes of $WO_3 \cdot H_2O$.

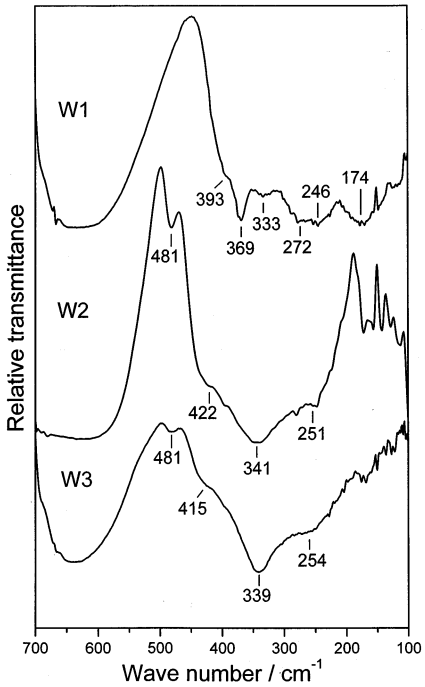

Fig. 8. Fourier transform infrared spectra of samples W1, W2 and W3 recorded in the far-IR region at room temperature. Specimens were pressed into the polyethylene matrix.

In the FT-IR spectrum of sample W2 two shoulders at 3582 and 3543 cm^{-1} are due to OH^- stretching vibrations. An additional IR band due to structural water is observed at 1602 cm^{-1}. A very strong and broad band at 820 cm^{-1} can be ascribed to ν(W=O) vibrations, whereas the shoulders at 754 and 660 cm^{-1} can be ascribed to ν(O–W–O) vibrations. A similar spectrum was recorded for sample W3 with a characteristic IR band at 817 cm^{-1} and shoulders at 715 and 660 cm^{-1}. In the far-IR region, for sample W2, a very strong IR band at 341 cm^{-1} with shoulders at 422 and 251 cm^{-1} was recorded (Fig. 8).

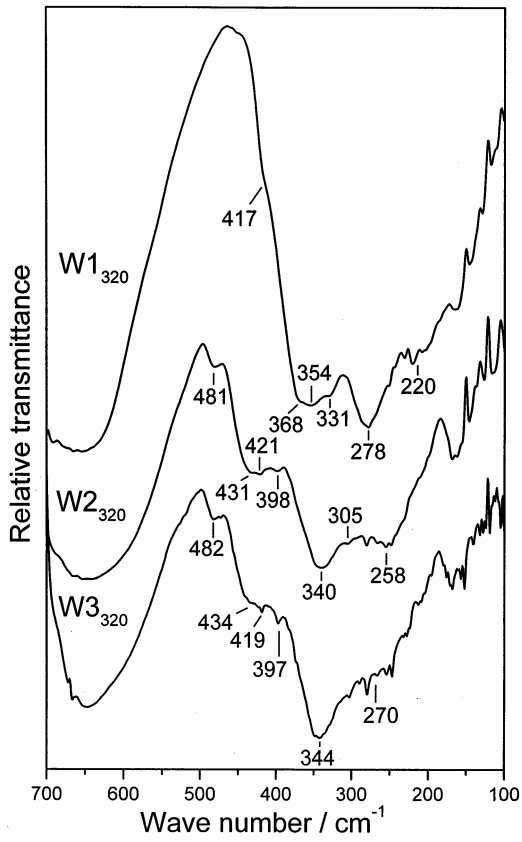

Fig. 10. Fourier transform infrared spectra of samples $W1_{320}$, $W2_{320}$ and $W3_{320}$ recorded in the far-IR region at room temperature. Specimens were pressed into the polyethylene matrix.

After heating sample W1 at 320°C, the corresponding FT-IR spectrum of the produced sample ($W1_{320}$) changed in relation to the spectrum of sample W1. A

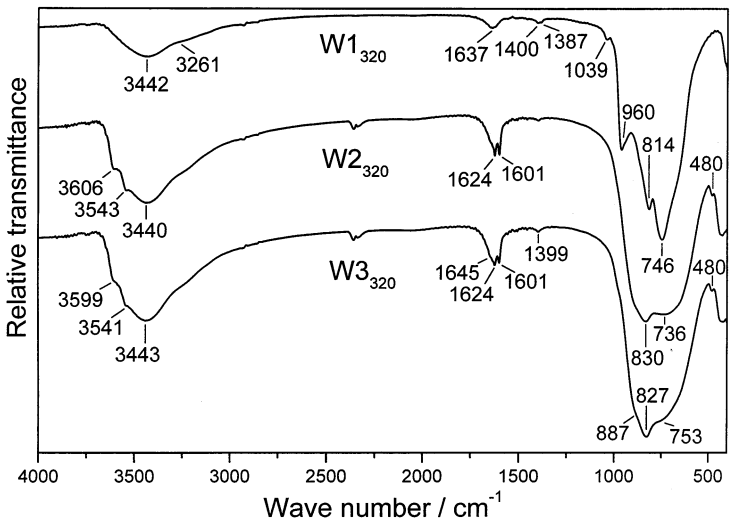

Fig. 9. Fourier transform infrared spectra of samples $W1_{320}$, $W2_{320}$ and $W3_{320}$ recorded at room temperature. Specimens were pressed into the KBr matrix.

very strong and broad band at 746 cm^{-1} associated with two IR bands at 814 and 960 cm^{-1}, is observed (Fig. 9), whereas in the far-IR region the main IR bands were centered at 354 and 278 and 220 cm^{-1} (Fig. 10). After heating samples W2 and W3 at 320°C the main spectral features of these samples were preserved, thus indicating that the structural changes observed for sample W1 upon its heating at 320°C, did not occur in the case of samples W2 and W3.

4. Conclusions

Tungsten trioxide hydrates were synthesized by (a) cation exchange reaction from sodium tungstate solution and (b) addition of HCl solution into sodium tungstate solution. A complete synthesis procedure is given, because the structural and other properties of the end products are highly dependent on the synthesis conditions.

An XRD pattern of the sample produced by cation exchange reaction corresponded to $WO_3 \cdot H_2O$. On heating this sample at 320°C the phase transition $WO_3 \cdot H_2O \rightarrow WO_3$ occurred. On the other hand, XRD patterns of the samples precipitated by the addition of HCl solution to the sodium tungstate solution corresponded to $WO_3 \cdot 0.33H_2O$, and the same crystal phase was preserved on heating these samples at 320°.

The DTA curve of the $WO_3 \cdot H_2O$ sample showed an endothermic peak at 265°C indicating a release of structural water, whereas a small exothermic peak at 315°C can be ascribed to the phase transition $WO_3 \cdot H_2O \rightarrow WO_3$. A good agreement between the theoretical (7.20 wt.%) and observed TGA weight loss (6.63 wt.%) was found for the $WO_3 \cdot H_2O$ sample. DTA curves of $WO_3 \cdot 0.33H_2O$ samples showed two exothermic peaks at 480 and 490°C due to the phase transition $WO_3 \cdot 0.33H_2O \rightarrow WO_3$, and one small endothermic peak at 735°C. For samples W2 and W3 TGA measurements showed a weight loss of 5.72 and 6.29 wt.%, respectively, which is much higher than the formula $WO_3 \cdot 0.33H_2O$ would permit. This effect can be explained by the presence of an amorphous fraction and/or poor crystalline $WO_3 \cdot 0.33H_2O$ phase with relatively abundant water content.

The Raman spectrum of the $WO_3 \cdot H_2O$ sample showed a sharp band at 942 cm^{-1} a very strong and broad band at 630 cm^{-1}, and a small intensity band at 346 cm^{-1}. After heating $WO_3 \cdot H_2O$ at 320°C the band at 942 cm^{-1} disappeared and two separate bands at 802 and 710 cm^{-1} appeared. A shoulder at 606 cm^{-1} suggested that the phase transition $WO_3 \cdot 0.33H_2O \rightarrow WO_3$ was not completed. The Raman spectra of the $WO_3 \cdot 0.33H_2O$ samples showed the most prominent band at 802 cm^{-1}. After heating the $WO_3 \cdot 0.33H_2O$ samples (W2 and W3) at 320°C the same spectral features of the Raman spectra were preserved. However, the spectral lines were better pronounced than for the starting samples, thus indicating a better crystallinity of the $WO_3 \cdot 0.33H_2O$ samples; this can be related to the XRD and DTA/TGA measurements. The FT-IR spectra also monitored structural changes in the prepared samples both in the mid-IR and far-IR regions. The FT-IR spectra clearly indicated the phase transition $WO_3 \cdot H_2O \rightarrow WO_3$, and preserved the same spectral features in case of the $WO_3 \cdot 0.33H_2O$ samples in accordance with complementary Raman spectra. The FT-IR spectra of the $WO_3 \cdot 0.33H_2O$ samples showed two IR bands at 1623 and 1602 cm^{-1} in the bending region of H_2O molecules, which seems to be related to the increase in the water content in samples W2 and W3 as shown by TGA. Generally, the structural water in tungsten trioxide plays a very important role in its photochromic behavior.

Acknowledgements

The authors wish to thank Dr Rudolf Trojko for his help in the thermal analysis work.

References

[1] J.P. Cronin, D.J. Tarico, J.C.L. Tonazzi, A. Agrawal, S.R. Kennedy, Sol. Energy Mater. Sol. Cells 29 (1993) 371.
[2] A. Agrawal, J.P. Cronin, R. Zhang, Sol. Energy Mater. Sol. Cells 31 (1993) 9.
[3] J. Arakaki, R. Reyes, M. Horn, W. Estrada, Sol. Energy Mater. Sol. Cells 37 (1995) 33.
[4] A. Azens, A. Hjelm, D. Le Bellac, C.G. Granqvist, J. Bawzynska, E. Pentjuss, J. Gabrusenoks, J.M. Wills, Solid State Ionics 86-88 (Part 2) (1996) 943.
[5] J. Livage, G. Guzman, Solid State Ionics 84 (1996) 205.
[6] M.A. Aegerter, C.O. Avellaneda, A. Pawlicka, M. Atik, J. Sol-Gel Sci. Technol. 8 (1997) 689.
[7] N. Özer, Thin Solid Films 304 (1997) 310.
[8] B. Munro, P. Conrad, S. Krämer, H. Schmidt, P. Zapp, Sol. Energy Mater. Sol. Cells 54 (1998) 131.
[9] B. Munro, S. Krämer, P. Zapp, H. Krug, J. Sol-Gel Sci. Technol. 13 (1998) 673.
[10] P. Judeinstein, J. Livage, J. Chim. Phys. Phys.-Chim. Biol. 90 (1993) 1137.
[11] M.M. Ostromecki, L.J. Burcham, I.E. Wachs, N. Ramani, J.G. Ekerdt, J. Mol. Catal. A Chem. 132 (1998) 43.
[12] M.M. Ostromecki, L.J. Burcham, I.E. Wachs, J. Mol. Catal. A Chem. 132 (1998) 59.
[13] J. Engweiler, J. Harf, A. Baiker, J. Catal. 159 (1996) 259.
[14] G. Ramis, G. Busca, C. Cristiani, L. Lietti, P. Forzatti, F. Bregani, Langmuir 8 (1992) 1744.
[15] A. Gutiérrez-Alejandre, J. Ramirez, G. Busca, Langmuir 14 (1998) 630.
[16] S.R. Vaudagna, R.A. Comelli, N.S. Figoli, Appl. Catal. A Gen. 164 (1997) 265.
[17] S. Colque, E. Payen, P. Grange, J. Mater. Chem. 4 (1994) 1343.
[18] C. Martin, P. Malet, G. Solana, V. Rives, J. Phys. Chem. B 102 (1998) 2759.

[19] L.J. Legore, K. Snow, J.D. Galipeau, J.F. Vetelino, Sens. Actuators B 35 (1996) 164.
[20] M. Ivanda, K. Furić, Appl. Optics 31 (1992) 6371.
[21] Powder Diffraction File, International Center for Diffraction Data, Newtown Square, PA, USA.
[22] T. Nishide, F. Mizukami, Thin Solid Films 259 (1995) 212.
[23] C. Li, H. Zhang, K. Wang, Y. Miao, Q. Xin, Appl. Spectrosc. 47 (1993) 56.
[24] S. Musić, A. Vértes, G.W. Simmons, I. Czakó-Nagy, H. Leidheiser Jr., J. Coll. Interface Sci. 85 (1982) 256.
[25] M. Gotić, S. Popović, N. Ljubeŝić, S. Musić, J. Mater. Sci. 29 (1994) 2474.
[26] L. Seguin, M. Figlarz, J. Pannetier, Solid State Ionics 63-65 (1993) 437.
[27] M. Figlarz, Prog. Solid State Chem. 19 (1989) 1.
[28] S. Laruelle, M. Figlarz, J. Solid State Chem. 111 (1994) 172.
[29] E. Cazzanelli, C. Vinegoni, G. Mariotto, A. Kuzmin, J. Purans, J. Solid State Chem. 143 (1999) 24.
[30] T. Vogt, P.M. Woodward, B.A. Hunter, J. Solid State Chem. 144 (1999) 309.
[31] P.M. Woodward, A.W. Sleight, T. Vogt, J. Solid State Chem. 131 (1997) 9.
[32] M.F. Daniel, B. Desbat, J.C. Lassegues, B. Gerand, M. Figlarz, J. Solid State Chem. 67 (1987) 235.
[33] M. Ivanda, S. Musić, M. Gotić, A. Turković, A.M. Tonejc, O. Gamulin, J. Mol. Struct. 480–481 (1999) 641.
[34] E. Salje, Acta Crystallogr. Sect. A 31 (1975) 360.
[35] T. Wadayama, H. Wako, A. Hatta, Mater. Trans. JIM 37 (1996) 1486.
[36] R. Martin Villarica, F. Nash, J. Chaiken, J. Osman, R. Bussjager, Mater. Res. Soc. Symp. Proc. 397 (1996) 347.
[37] I. Shiyanovskaya, H. Ratajczak, J. Baran, M. Marchewka, J. Mol. Struct. 348 (1995) 99.
[38] I. Shiyanovskaya, M. Hepel, J. Electrochem. Soc. 145 (1998) 1023.